

References

1. Punyagupta S, Juttijudata P, Bunnag T. Eosinophilic meningitis in Thailand. Clinical studies of 484 typical cases probably caused by *Angiostrongylus cantonensis*. *Am J Trop Med Hyg* 1975;24:921–931.
2. Jindrak K. *Angiostrongylus cantonensis* (eosinophilic meningitis, Alicata's disease). *Contemp Neurol Ser* 1975;12:133–164.
3. Koo J, Pien F, Kliks M. *Angiostrongylus* (*Parastrostrongylus*) eosinophilic meningitis. *Rev Infect Dis* 1988;10:1155–1162.
4. Procriv P, Spratt D, Carlisle M. Neuro-angiostrongyliasis: unresolved issues. *Int J Parasitol* 2000;30:1295–1303.
5. Vejajiva A. Parasitic diseases of the nervous system in Thailand. *Clin Exp Neurol* 1978;15:92–97.
6. Kuberski T, Wallace G. Clinical manifestations of eosinophilic meningitis due to *Angiostrongylus cantonensis*. *Neurology* 1979;29:1566–1570.
7. Schmutzhard E, Boongird P, Vejajiva A. Eosinophilic meningitis and radiculomyelitis in Thailand, caused by CNS invasion of *Gnathostoma spinigerum* and *Angiostrongylus cantonensis*. *J Neurol Neurosurg Psychiatry* 1988;51:80–87.
8. Dooley J, Neafe R. *Angiostrongylus cantonensis* infections. In: Binford C, Connor D, eds. *Pathology of tropical and extraordinary diseases*. Washington, DC: Armed Forces Institute of Pathology, 1976:446–451.
9. Hwang K, Chen E. Clinical studies on angiostrongyliasis cantonensis among children in Taiwan. *Southeast Asian J Trop Med Public Health* 1991;22(suppl):194–199.
10. Tsai H, Liu Y, Kunin C, et al. Eosinophilic meningitis caused by *Angiostrongylus cantonensis*: report of 17 cases. *Am J Med* 2001;111:109–114.
11. Cooke-Yarborough C, Kornberg A, Hogg G, et al. A fatal case of angiostrongyliasis in an 11-month-old infant. *Med J Aust* 1999;170:541–543.
12. Witoonpanich R, Chuahirun S, Soranastaporn S, Rojanasunan P. Eosinophilic myelomeningoencephalitis caused by *Angiostrongylus cantonensis*: a report of three cases. *Southeast Asian J Trop Med Public Health* 1991;22:262–267.
13. Kliks M, Kroenke K, Hardman J. Eosinophilic radiculomyeloencephalitis: an angiostrongyliasis outbreak in American Samoa related to ingestion of *Achatina fulica* snails. *Am J Trop Med Hyg* 1982;31:1114–1122.
14. Wood G, Delamont S, Whitby M, Boyle R. Spinal sensory radiculopathy due to *Angiostrongylus cantonensis* infection. *Postgrad Med J* 1991;67:70–72.
15. Pipitgool V, Sithithaworn P, Pongmuttasaya P, Hinz E. *Angiostrongylus* infections in rats and snails in northeast Thailand. *Southeast Asian J Trop Med Public Health* 1997;28(suppl 1):190–193.
16. Waisberg J, Corsi C, Rebelo M, et al. Jejunal perforation caused by abdominal angiostrongyliasis. *Rev Inst Med Trop Sao Paulo* 1999;41:325–328.
17. Limaye L, Bhopale M, Renapurkar D, Sharma K. The distribution of *Angiostrongylus cantonensis* (Chen) in the central nervous system of laboratory rats. *Folia Parasitol (Praha)* 1983;30:281–284.
18. Yii C. Clinical observations on eosinophilic meningitis and meningoencephalitis caused by *Angiostrongylus cantonensis* on Taiwan. *Am J Trop Med Hyg* 1976;25:233–249.
19. Punyagupta S, Bunnag T, Juttijudata P. Eosinophilic meningitis in Thailand. Clinical and epidemiological characteristics of 162 patients with myeloencephalitis probably caused by *Gnathostoma spinigerum*. *J Neurol Sci* 1990;96:241–256.
20. Kuberski T, Bart R, Briley J, Rosen L. Recovery of *Angiostrongylus cantonensis* from cerebrospinal fluid of a child with eosinophilic meningitis. *J Clin Microbiol* 1979;9:629–631.
21. Nelson R, Warren R, Scotti F, et al. Ocular angiostrongyliasis in Japan: a case report. *Am J Trop Med Hyg* 1988;38:130–132.
22. Nishimura K, Hung T. Current views on geographic distribution and modes of infection of neurohelminthic diseases. *J Neurol Sci* 1997;145:5–14.

Microscopic R2* Mapping of Reduced Brain Iron in the Belgrade Rat

Holly A. Zywicke, BS,¹ Peter van Gelderen, PhD,² James R. Connor, PhD,³ Joseph R. Burdo, BS,³ Michael D. Garrick, PhD,⁴ Kevin G. Dolan, BS,⁴ Joseph A. Frank, MD,¹ and Jeff W. M. Bulte, PhD¹

R2* mapping has recently been used to detect iron overload in patients with movement disorders. We demonstrate here that this technique can also be used to detect reduced brain iron, as in the case of a missense mutation in the iron-transporting protein divalent metal transporter 1. Surprisingly, we found that the same brain regions are affected (ie, the globus pallidus, substantia nigra, and cerebellar dentate nucleus); this suggests a much more extensive role for these structures in regulating overall brain iron homeostasis. Therefore, for the clinical monitoring of movement disorders for which normal brain iron homeostasis (either overload or reduction) may be implicated, R2* mapping appears to be well-suited.

Ann Neurol 2002;52:102–105

In the brain, iron is an essential element for basic cellular processes such as myelination, neurotransmitter production, and adenosine triphosphate synthesis. Evidence has now accumulated¹ for an association be-

From the ¹Laboratory of Diagnostic Radiology Research, Clinical Center, and ²Laboratory of Advanced Magnetic Resonance Imaging, National Institute of Neurological Diseases and Stroke, National Institutes of Health, Bethesda, MD; ³Department of Neuroscience and Anatomy, Pennsylvania State University, Hershey, PA; and ⁴Department of Biochemistry, State University of New York, Buffalo, NY.

Received Oct 30, 2001, and in revised form Feb 15, 2002. Accepted for publication Feb 15, 2002.

Address correspondence to Dr Bulte, Department of Radiology, Johns Hopkins University School of Medicine, 217 Traylor Building, 720 Rutland Avenue, Baltimore, MD 21205-2195.
E-mail: jwmbulte@mri.jhu.edu

tween excess brain iron and a number of common neurodegenerative disorders, such as Parkinson's disease, Huntington's disease, Friedreich's ataxia, Alzheimer's disease, epilepsy, Hallervorden-Spatz disease,² and neuroferritinopathy.³ Elucidating the exact biochemical pathways of brain iron delivery, uptake, and intracerebral transport is of paramount importance for a better understanding of the role of iron in the underlying pathologies of these disorders.

It is currently believed that iron transport to the brain is mediated by transferrin and the transferrin receptor. Upon the endocytosis of transferrin-iron-transferrin receptor and the release of iron in the acidic endosomes, iron is translocated to the cellular cytoplasm by divalent metal transporter 1 (DMT1).⁴ At present, very little is known about intracerebral intercellular iron transport beyond the endothelium. The Belgrade (*b/b*) rat⁵ has a G185R mutation in DMT1, resulting in hypochromic, microcytic anemia with the presence of mitochondria that contain less iron.⁶ Less iron gets to mitochondria because of a defect in the exit of iron from endosomes during the transferrin cycle.⁷ The defect also affects transferrin-independent iron uptake in the intestinal tract⁸ and elsewhere.⁹ The *b/b* rat model has, therefore, been used to determine the effect of inactive DMT1 on cellular iron distribution in the brain.¹⁰ It has been determined that Belgrade rats have fewer and less dense iron-positive pyramidal neurons and oligodendrocytes, indicating the importance of DMT1 in maintaining normal brain iron homeostasis and suggesting a role for brain iron acquisition.

Although these and other reports rely on traditional histochemical staining techniques for the detection of iron (ie, diaminobenzidine-enhanced Perls' reaction), recent advances in magnetic resonance imaging have shown that it is possible to detect iron noninvasively. The antiferromagnetic Fe(III) oxyhydroxide cores of the protein ferritin form local microscopic field inhomogeneities that enable faster T2 and T2* proton relaxation. On standard spin-echo and gradient-echo magnetic resonance imaging sequences, the net result is an area of hypointensity for the iron-containing tissue, but in general these methods are prone to artifacts, lack specificity for iron (other tissue components may cause hypointensity), and are semiquantitative at best. The rate of the transverse relaxation, R2, is proportional to the local iron concentration and increases linearly with the field. Therefore, the field-dependent R2 increase may be used as a specific parameter for the quantification of tissue iron,^{11,12} but its clinical use requires at least two instruments. R2* refers to T2 relaxation without pulse compensation for proton dephasing that occurs in the vicinity of microscopic field gradients, and it is most sensitive to the presence of iron. Although other tissue components may contribute to R2*, R2*

mapping has recently been used to detect brain iron overload in the basal ganglia of patients with Parkinson's disease¹³ and in the cerebellar dentate nucleus in Friedreich's ataxia.¹⁴ Although this technique has been proven to be able to detect excess brain iron, its suitability for detecting diminished brain iron (eg, for the Belgrade rat) remains unproven. We report here that R2* mapping may also be used to provide uniquely sensitive and quantitative information about reduced brain iron.

Materials and Methods

Brains from *b/b* Fischer/Wistar rats, ages 26 to 28 months ($n = 3$), and age-matched *+/+* littermate wild-type controls ($n = 3$) were perfused with 4% paraformaldehyde and placed in 12ml syringes filled with a perfluoropolyether (devoid of proton signals). Three-dimensional, multigradient-echo magnetic resonance images were obtained at a 104 μ m isotropic resolution with a 4.7T Varian INOVA NMR spectrometer (Palo Alto, CA) and a DOTY Litz coil 25mm in diameter. The scan parameters were as follows: field of view, 30 \times 20 \times 20mm; matrix, 288 \times 192 \times 192; number of excitations, 12; repetition time, 100msec; echo time, 6msec; number of echoes, 6; and flip angle, 15 degrees. Interactive Data Language (IDL) processing software was then used to create images from the three-dimensional data set. From the amplitude images of each different echo, R2* maps were calculated by the fitting of an exponential decay to every voxel with sufficient intensity.

For each region of interest in both hemispheres, the average R2* from three adjacent slices was calculated with a fixed number (n) of pixels. This was done for the globus pallidus ($n = 425$), substantia nigra ($n = 200$), dentate nucleus ($n = 225$), normal cortical gray matter ($n = 325$), and normal white matter (ventral hippocampal commissure, $n = 250$). The mean R2* values for both hemispheres were used because the difference between the two sites was less than or equal to 5%. R2* data were analyzed for statistical significance with a two-tailed Student t test.

Results

Figure 1 shows the R2* maps of mutant animals versus wild-type animals. For histopathological correlation, a side-by-side comparison is shown for deparaffinated 10 μ m tissue sections stained for ferric iron with a diaminobenzidine-enhanced Perls' reaction. R2* maps are shown as intensity maps; that is, areas with higher R2* values (more iron) display higher signal intensity.

To obtain quantitative information on the relative amount of iron, we calculated the average R2* for each region of interest. Figure 2 shows a striking and significant ($p < 0.001$) difference between the two groups for the globus pallidus, substantia nigra, and dentate nucleus, whereas normal gray and white matter were not affected ($p > 0.05$).

Discussion

We were surprised to observe that the same brain regions commonly reported to be involved in iron over-

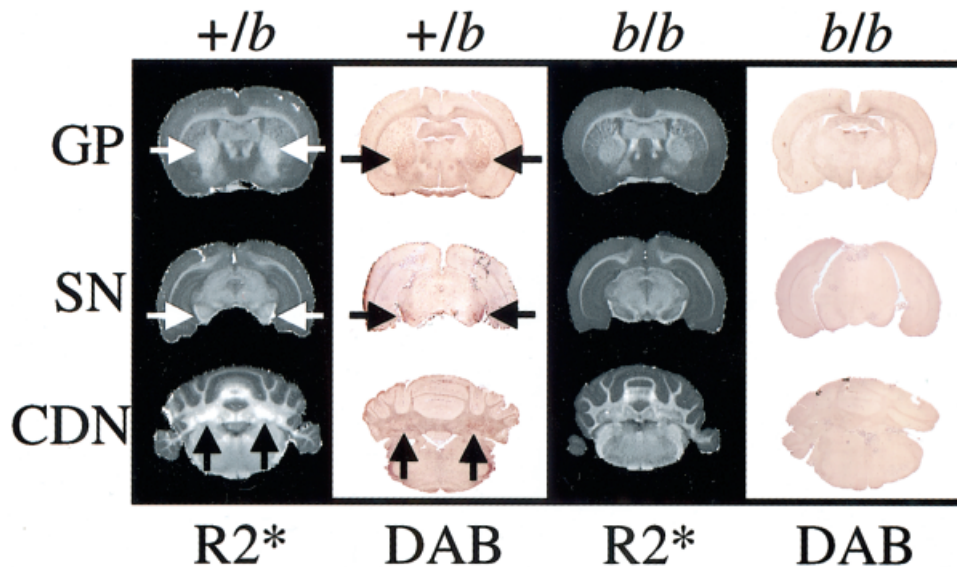


Fig 1. Microscopic R2* maps and diaminobenzidine (DAB)-enhanced Prussian blue stains of +/b wild-type control and b/b rats. Arrows indicate the outline of the globus pallidus (GP), substantia nigra (SN), and cerebellar dentate nucleus (CDN).

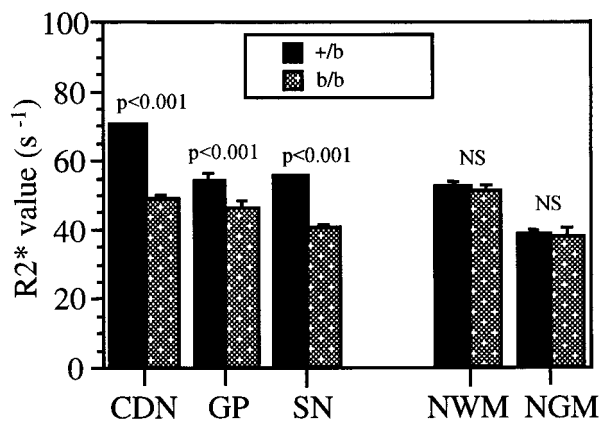
load (the globus pallidus, substantia nigra, and dentate nucleus) are apparently also specifically implicated in iron reduction due to impaired DMT1. This parallel implicates these regions in a much more extensive role in regulating overall brain iron homeostasis, serving not only as a well-established depot for storing excess iron but also as centers that become depleted when intracellular (endosomal) DMT1-dependent iron trafficking is blocked. It is at present unclear whether this is the direct result of reduced iron uptake in these regions; it could also result from an increased demand for iron from other areas of the brain, which could accelerate depletion. In Belgrade rats, there is a decrease in im-

munodetectable DMT1 on endothelial cells in comparison with normal rats.¹⁵

It is noteworthy that R2* mapping of patients with restless legs syndrome recently indicated significantly decreased R2* values in the substantia nigra and to a lesser extent in the putamen, which was speculated to be the result of brain iron insufficiency.¹⁶ This study shows a direct, specific correlation between reduced brain iron content and R2* values. Of further significance is our observation that, contrary to the results of a clinical restless legs syndrome study,¹⁶ there was a significant reduction in R2* values of the dentate nucleus in Belgrade rats. Our studies were carried out at a higher field strength (4.7T) than that of most clinical scanners (3.0 and 1.5T), and because 1/T2 of ferritin increases linearly with the field,¹⁷ this higher field strength may be more sensitive in detecting the presence of iron. Our data clearly indicate that Belgrade rats should be carefully observed for any symptoms associated with restless legs syndrome, and that it should also be determined whether DMT1 expression and iron transport are compromised in restless legs syndrome patients.¹⁸ Therefore, we believe that this rat model may serve as a basis for further study of this prevalent movement disorder, which affects between 5 and 15% of adults.^{19,20}

In summary, these results demonstrate that magnetic resonance imaging in conjunction with R2* mapping can be used to pinpoint, with microscopic precision, tissue areas that are most affected by a missense mutation in the iron-transporting protein DMT1. In addition to detecting iron overload, R2* mapping may, therefore, also be used to visualize reduced brain iron,

Fig 2. Calculated average R2* values for the globus pallidus (GP), substantia nigra (SN), and cerebellar dentate nucleus (CDN) of +/b and b/b rats. The R2* values for the unaffected areas of normal white matter (NWM) and gray matter (NGM) are shown as internal controls.



opening the door to noninvasive monitoring of brain iron homeostasis at regional and cellular levels. Because this can be done noninvasively and serially (repeatedly over time), this technique appears well suited for the clinical monitoring of movement disorders for which normal brain iron homeostasis may be implicated, be it an excess or insufficiency.

References

1. Thompson KJ, Shoham S, Connor JR. Iron and neurodegenerative diseases. *Brain Res Bull* 2001;55:155–164.
2. Zhou B, Westaway SK, Levinson B, et al. A novel pantothenate kinase gene (PNK2) is defective in Hallervorden-Spatz syndrome. *Nat Genet* 2001;28:345–349.
3. Curtis ARJ, Fey C, Morris CM, et al. Mutation in the gene encoding ferritin light polypeptide causes dominant adult-onset basal ganglia disease. *Nat Genet* 2001;28:350–354.
4. Fleming MD, Romano MA, Su MA, et al. Nramp2 is mutated in the anemic Belgrade (b) rat: evidence of a role for Nramp2 in endosomal iron transport. *Proc Natl Acad Sci U S A* 1998;95:1148–1153.
5. Sladic-Simic D, Zivkovic N, Pavic D, et al. Hereditary hypochromic microcytic anemia in the laboratory rat. *Genetics* 1966;53:1079–1089.
6. Garrick LM, Gniecko K, Liu Y, et al. Iron distribution in Belgrade rat reticulocytes after inhibition of heme synthesis with succinylacetone. *Blood* 1993;81:3414–3421.
7. Garrick MD, Gniecko K, Liu Y, et al. Transferrin and the transferrin cycle in Belgrade rat reticulocytes. *J Biol Chem* 1993;268:14867–14874.
8. Oates PS, Morgan EH. Defective iron uptake by the duodenum of Belgrade rats fed diets of different iron contents. *Am J Physiol Gastrointest Liver Physiol* 1996;270:G826–G832.
9. Garrick LM, Dolan KG, Romano MA, Garrick MD. Non-transferrin-bound iron uptake in Belgrade and normal rat erythroid cells. *J Cell Physiol* 1999;178:349–358.
10. Burdo JR, Martin J, Menzies SL, et al. Cellular distribution of iron in the brain of the Belgrade rat. *Neuroscience* 1999;93:1189–1196.
11. Bartzokis G, Aravagiri M, Oldendorf WH, et al. Field-dependent transverse relaxation rate increase may be a specific measure of tissue iron stores. *Magn Reson Med* 1993;29:459–464.
12. Bulte JW, Miller GM, Vymazal J, et al. Hepatic hemosiderosis in non-human primates: quantification of liver iron using different field strengths. *Magn Reson Med* 1997;37:530–536.
13. Ye FQ, Martin WRW, Allen PS. Estimation of brain iron in vivo by means of the interecho time dependence of image contrast. *Magn Reson Med* 1996;36:153–158.
14. Waldvogel D, van Gelderen P, Hallett M. Increased iron in the dentate nucleus of patients with Friedreich's ataxia. *Ann Neurol* 1999;46:123–125.
15. Burdo JR, Menzies SL, Simpson IA, et al. Distribution of divalent metal transporter 1 and metal transport protein 1 in the normal and Belgrade rat. *J Neurosci Res* 2001;66:1198–1207.
16. Allen RP, Barker PB, Wehrli F, et al. MRI measurement of brain iron in patients with restless legs syndrome. *Neurology* 2001;56:263–265.
17. Vymazal J, Brooks RA, Zak O, et al. T1 and T2 of ferritin at different field strengths: effect on MRI. *Magn Reson Med* 1992;27:368–374.
18. Earley CJ, Allen RP, Beard JL, Connor JR. Insight into the pathophysiology of restless legs syndrome. *J Neurosci Res* 2000;62:623–628.
19. Lavigne GJ, Montplaisir JY. Restless legs syndrome and sleep bruxism: prevalence and association among Canadians. *Sleep* 1994;17:739–743.
20. Phillips B, Young T, Finn L, et al. Epidemiology of restless legs symptoms in adults. *Arch Intern Med* 2000;160:2137–2141.

Preferential Loss of Paternal 19q, but Not 1p, Alleles in Oligodendrogliomas

Marc Sanson, MD, PhD,^{1,2} Pascal Leuraud, MSc,² Yannick Marie, MSc,² Jean-Yves Delattre, MD,^{1,2} and Khê Hoang-Xuan, MD^{1,2}

Portions of chromosomes 1p and 19q, which are frequently deleted in oligodendrogliomas, are subject to genomic imprinting, suggesting that the putative tumor suppressor genes could be monoallelically expressed. The parental origins of 1p and 19q allele losses were determined in 6 cases of pure oligodendroglioma. An equilibrated parental loss (3 maternal and 3 paternal) was found for 1p deletions. In contrast, 19q deletions always occurred on the paternal copy ($p = 0.015$). In this setting, a cloning strategy based on a search for homozygous deletion or mutation of the remaining allele would be appropriate for identifying the tumor suppressor gene located on 1p but inappropriate for identifying the presumably monoallelically expressed tumor suppressor gene located on 19q.

Ann Neurol 2002;52:105–107

Combined losses of 1p and 19q chromosomes occur in 50 to 70% of patients with oligodendroglioma. This finding is important, not only as a diagnostic marker of oligodendroglioma but also as an indicator of higher chemosensitivity and prolonged survival.¹ Strategies for cloning the putative tumor suppressor genes located on these chromosomes are being developed, based on a search for homozygous deletion or mutation of the remaining allele. However, this approach may not be

From ¹Fédération Neurologique Mazarin and ²Unité INSERM U495, Hôpital de la Salpêtrière, Université Pierre et Marie Curie, Paris, France.

Received Jan 2, 2002, and in revised form Feb 15. Accepted for publication Feb 15, 2002.

Address correspondence to Dr Sanson, Fédération Neurologique Mazarin, Hôpital de la Salpêtrière, 47 Bd de l'Hôpital, 75013 Paris, France. E-mail: m.sanson@psl.ap-hop-paris.fr